

CLIQUE: Spatiotemporal Object Re-identification at the City Scale

Tiantu Xu
Purdue ECE

Kaiwen Shen
Purdue ECE

Yang Fu
UIUC

Humphrey Shi
University of Oregon

Felix Xiaozhu Lin
University of Virginia

Abstract

Object re-identification (ReID) is a key application of city-scale cameras. While classic ReID tasks are often considered as image retrieval, we treat them as spatiotemporal queries for locations and times in which the target object appeared. Spatiotemporal reID is challenged by the accuracy limitation in computer vision algorithms and the colossal videos from city cameras. We present CLIQUE, a practical ReID engine that builds upon two new techniques: (1) CLIQUE assesses target occurrences by clustering fuzzy object features extracted by ReID algorithms, with each cluster representing the general impression of a distinct object to be matched against the input; (2) to search in videos, CLIQUE samples cameras to maximize the spatiotemporal coverage and incrementally adds cameras for processing on demand. Through evaluation on 25 hours of videos from 25 cameras, CLIQUE reached a high accuracy of 0.87 (*recall at 5*) across 70 queries and runs at 830 \times of video realtime in achieving high accuracy.

1 Introduction

City-scale camera deployment As video intelligence advances and camera cost drops, city cameras expand fast. Strategically deployed near key locations, such as highway entrances or road intersections, multiple cameras (reported to be 2–5 per location [41, 56]) offer complementary, often overlapped viewpoints of scenes.

Object ReID on city videos A key application of city cameras is object re-identification (ReID): given an input image of an object X, searching for occurrences of X in a video repository. ReID has been an important computer vision task, seeing popular use cases such as crime investigation and traffic planning [33, 41, 42]. Many ReID algorithms are proposed recently, fueled by neural networks [12, 13, 20, 54, 55, 65, 67, 68]. Object ReID over city videos is typically “finding a needle in haystack”. The queried videos are long and produced by many cameras; the videos may not contain the input image, or any images from the camera that produced the input image (called the *origin* camera); the occurrences of target object can be rare and transient. For instance, in a popular dataset of city

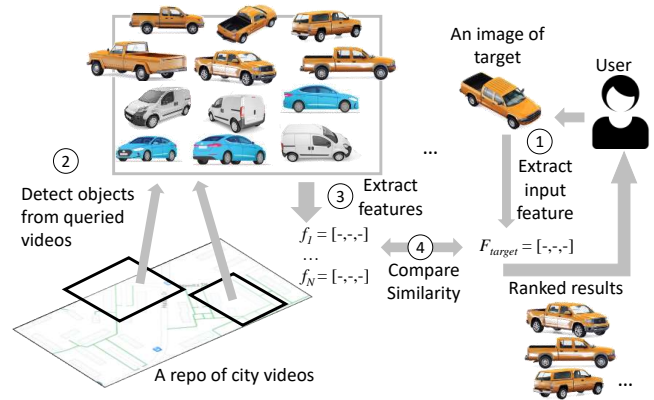


Figure 1: The classic pipeline for object ReID, formulated as image retrieval

traffic videos [56], 99% of vehicles only appear for less than 10 seconds.

The common pipeline structure for ReID is shown in Figure 1: (1) given an input image of target object X, the pipeline extracts its feature, e.g., using ResNet-152 [17] to extract a 1024-dimension vector [20, 55]; (2) from the queried videos, the pipeline detects all bounding boxes belonging to the same class as X, e.g., using YOLO [48]; (3) the pipeline extracts features of all detected bounding boxes; (4) it calculates pairwise similarities between X and the bounding boxes. The similarity is often measured as feature distance [40], where a shorter distance suggests a higher similarity between X and a bounding box. Of the four stages, stage 2 and 3 are most expensive. For instance, calculating feature distances in stage 4 is three orders of magnitude faster than extracting the features in stage 3. The cost of stage 2 and 3 further grows with the amount of videos. This pipeline structure is widely used, e.g., by almost all participants in popular vehicle ReID challenges [20, 38, 55].

Proliferating ReID algorithms call for a practical ReID system. Our driving use case is vehicle ReID, where personal identifiable information such as license plates are intentionally removed for privacy [56]. Vehicle ReID is considered one of

the most important ReID problems [42]. The techniques are likely transferable to other object classes.

Challenge 1: Limitations of modern ReID algorithms By its definition in computer vision, ReID focuses on differentiating numerous objects of the *same class*, e.g., cars. In real-world videos, however, many objects of the same class exhibit minor visual differences; yet bounding boxes of the same object – captured by the same or different cameras – may appear quite different. As we will show in Section 2, even sophisticated feature extractors may deem bounding boxes of *different* objects more similar than bounding boxes of the *same* object.

Challenge 2: Many cameras, large videos City cameras can be numerous. With 2-5 cameras per intersection [41, 56] and 60–500 intersections per square mile in urban areas [11], a query covering a few square miles would need to process a few hundred, if not a few thousand, cameras. Furthermore, modern ReID pipelines have an insatiable need for resources. For example, Titan V, a \sim \\$3,000 modern GPU, runs YOLO [49, 50] for detecting bounding boxes at only 40 FPS. The GPU running ResNet-152 extracts \sim 80 features per second. To process city videos from one square mile in a day, we estimate at least several hundred GPU hours are needed. This cost quickly becomes prohibitive as camera deployment and query scope expands. Resorting to cheap vision algorithms, e.g. smaller neural networks or SIFT, is unlikely to help: they are much more susceptible to subtle visual differences and disturbance, making ReID results even less usable.

Principles While prior research formulates ReID as image retrieval queries, i.e., to find every bounding box of a target object X [20, 23, 24, 55], we treat ReID as *spatiotemporal* queries, which search for what users care about: the times and locations in which object X appeared. This gives opportunities to overcome the accuracy limitation on individual bounding boxes, and to quickly emit times and locations before processing all bounding boxes in the queried videos.

We address the multitude of city cameras by renewing a wisdom in video analytics: resource/quality tradeoffs [18, 25, 29, 61, 63]. Prior video systems often target fewer cameras, making such tradeoffs *within* a video stream, e.g., by tuning frame resolutions, rates, and cropping factors. On city-scale videos, however, processing more cameras is almost always favorable than processing more pixels from each camera. This is because: (1) cameras in different locations provide extensive spatial coverage; (2) cameras in the same location provide complementary viewpoints. Both factors benefit ReID queries more than video quality. To this end, we prioritize increasing camera coverage over increasing video quality, e.g., frame rate and resolution.

We make minimum, qualitative assumptions on camera deployment. Quantitative deployment knowledge, e.g., camera orientations and correlations, used to enable optimizations within smaller camera networks [24]. For emerging city-scale

cameras, however, it is unclear if there exists a generic, quantitative deployment model. Minimizing assumptions allow a generic system design, which, as we will demonstrate, serves as the basis for deployment-specific optimizations.

CLIQUE We present a ReID engine called CLIQUE. Catering to spatiotemporal queries, CLIQUE organizes all videos in a repository as spatiotemporal cells, where a cell $\langle L, T \rangle$ contains video clips captured by all cameras near a geo-location L during a time period T . CLIQUE answers a query for target object X with a short list of spatiotemporal cells, ranked by their promises of containing X ; each returned cell is accompanied by video clips, with annotations of the likely bounding boxes of X . As executing a query, CLIQUE keeps updating the rank based on new results from video processing. The user reviews returned cells and makes the final decision.

We design and evaluate CLIQUE as a recall-oriented system [4]: it seeks to find all positive cells (which are rare) and rank them to the top. As such, CLIQUE minimizes human efforts in analyzing videos; it does not seek to replace humans, whose knowledge cannot (yet) be substituted by algorithms on real-world videos. This goal is shared by existing recall-oriented systems, e.g., for legal documents or patents search [3, 5], where final decisions from humans are indispensable.

Key design 1: clustering fuzzy bounding boxes From a set of bounding boxes, how should CLIQUE assess occurrences of a target object with confidence? Our insight is: how is an object perceived by a camera is heavily impacted by (1) the camera’s posture, including position and orientation; (2) transient disturbance, such as occlusion and background clutter. These impacts sometimes overshadow the object’s characteristics, e.g., shape and color.

To counter the two impacts, CLIQUE *matches* the origin camera’s posture: it samples diverse co-located cameras in hope of finding ones with postures similar to the input. CLIQUE *mitigates* the disturbance: it clusters similar bounding boxes captured by a camera during a period of time. Each resultant cluster thus represents the camera’s general “impression” of a distinct object. CLIQUE estimates the occurrence of X based on the similarity between the input image and distinct objects as represented by clusters. Clustering has been a classic algorithm in data processing [27, 28, 30] especially in vision [18]; CLIQUE is novel in applying it to ReID, deriving robust query answers from fuzzy bounding box features. Clustering suits our principle of prioritizing camera coverage, as it tolerates low frame rate on each camera.

Key design 2: Incremental search in spatiotemporal cells how to search in numerous spatiotemporal cells and quickly find target objects? The key is the camera sampling strategy: to avoid redundant video contents as much as possible while exploiting diverse camera postures as needed. CLIQUE navigates its resource spending towards cells where new discovery of target occurrences is most likely. To do this, CLIQUE

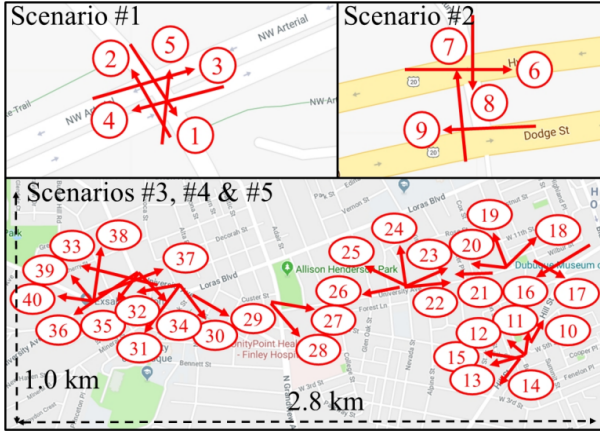


Figure 2: **An example of city camera deployment that motivates our design.** Each red arrow: a camera’s location (the arrow tail) and orientation (the arrow direction); Numbers: camera IDs. Both data and figure from CityFlow [56].

starts a query with a minimum number of cameras to quickly estimate promises of all cells; it processes videos from additional cameras for undecided cells; it iteratively assesses cell promises and re-ranks all cells for subsequent search.

We implement CLIQUE and evaluate it on a video dataset of 25 hours of videos from 25 cameras. On 70 queries with different target objects, CLIQUE delivers a high recall accuracy of 0.87 on average; it reaches high an accuracy goal of 0.99 in 108.5 seconds on average, at the speed of $830\times$ of video realtime. Compared to alternative designs, CLIQUE reduces query delays by up to $6.5\times$. We further evaluate deployment-specific optimizations.

Contributions We made the following contributions.

- Towards a practical ReID system, we advocate a new approach: focusing on finding relevant spatiotemporal cells rather than individual object instances.
- We present to cluster fuzzy bounding boxes as approximations of distinct objects, which effectively overcomes limitation in ReID algorithm accuracy.
- We present incremental search in cells. This minimizes redundant processing while exploiting diverse camera viewpoints, which reduces the ReID compute cost.
- We report CLIQUE, a ReID system that works on large video repositories.

Ethical considerations In this study: all visual data used is from the public domain; no information traceable to human individuals is collected or analyzed.

2 Motivations

2.1 System model

Queries & videos We target retrospective queries: at the query time, all videos are already stored in a central repository. We assume a large repository of videos from geo-distributed cameras. Preprocessing at ingestion, i.e., as videos are being captured, is optional, as permitted by compute resource. At ingestion time, the system knows the object classes that may be queried, e.g., cars, but not the input images of queries.

A query includes an input image of the target object X and the scope of videos to be queried; the query does not carry any metadata, e.g., a timestamp or the origin camera that produced the input image. Following the norm in ReID research [12, 13, 20, 54, 55, 68], we do not assume the video repository contains the input image; we do not assume any other images from the origin camera is available.

Cameras We make minimum, qualitative assumptions on camera deployment. The deployment covers multiple geo-locations. At each location, multiple cameras are co-located as a *geo-group*. The query system knows which cameras are co-located, i.e., belonging to the same geo-group. Of the same geo-group and during a short period of time, e.g., tens of seconds, cameras are likely (although not necessarily) to capture similar sets of objects from different viewpoints. A deployment example is shown in Figure 2.

We do not assume that the query system knows quantitative camera postures and quantitative correlations across camera geo-groups (e.g., “one object appearing in geo-group A has 50% chance to reappear in geo-group B within the next 10 minutes”). There is no sufficient evidence showing such knowledge is standard in city camera deployment. As such, we design a generic system without such knowledge, and evaluate how the resultant system can be augmented in case some knowledge becomes available (Section 7).

2.2 Challenge 1: Algorithm limitations

Observation: fuzzy bounding boxes Figure 3 compares the features of a target vehicle A and a confusing vehicle B. The features are extracted by ResNet-152, a state-of-the-art neural network. Given an image of vehicle A: (1) ResNet-152 deems 10% of B’s bounding boxes exhibit shorter feature distances than A’s, hence are more similar to the input image, as compared to A’s other bounding boxes; (2) the bounding box closest to the input image is from the confusing vehicle B but not A; (3) Bounding boxes of the same vehicle show a high variation, as reflected by the wide range of the feature distances. The above example of fuzzy bounding boxes is not isolated: they are the major hurdle for ReID accuracy, responsible for an average of 0.65 loss of accuracy in 20% of queries executed by a baseline design (Section 7).

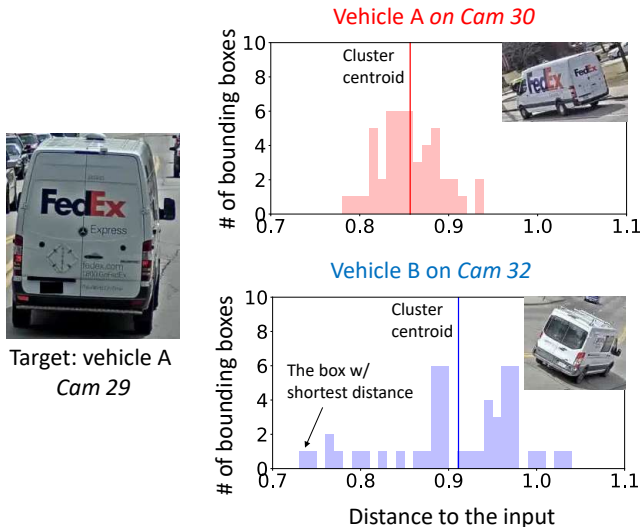


Figure 3: **Examples of fuzzy bounding boxes.** (Left) an image of vehicle A, whose feature is the input. (Top) a histogram of distances between the input and other features of A. (Bottom) a histogram of distances between the input and features of B, a confusing vehicle. All features are 1×1024 vectors extracted by ResNet-152. Euclidean distances with L-2 norm [40] are used. Video clips: 4.7/4.9 sec for vehicle A/B from CityFlow [56]

The causes Why fuzzy bounding boxes? We explain the root cause with a simple formula:

$$Cam'(X) = Cam(X) + \mathcal{N}$$

This formula describes how $Cam'(X)$, a camera’s actual observation of an object, is formed. X is the object’s inherent characteristics, e.g., its color, shape, skeleton, and key points. Two factors prevent a ReID system from directly learning X and matching it to the input. First, a camera’s posture modulates X as $Cam(X)$, i.e., the camera’s *ideal* observation on X . Second, the ideal observation is susceptible to transient disturbances \mathcal{N} , e.g., changes in resolution and viewpoint as objects move, background clutter, and occlusion. The impacts of camera postures and transient disturbances are strong, sometimes even stronger than the impact of inherent characteristics X . We have observed a different camera viewpoint of the same object resulting in $3 \times$ difference in feature distances. Hence, classic ReID pipelines that aim at labeling each bounding box are in fact deciding on $Cam'(X)$, which encodes the camera posture and also the disturbances. The pipelines cannot achieve high accuracy because it is difficult to model $Cam()$ and \mathcal{N} and eliminate their impacts accordingly.

2.3 Challenge 2: Numerous cameras & videos

Colossal data volume A city camera generates more than 6 GBs of videos daily (720P at 1FPS). Estimated from re-

cent reports on camera deployment in northern American cities [11, 41, 56], the number of city cameras per square mile ranges from a few hundred to a few thousand. A ReID query covering only a few square miles and one day of videos will have to consume PBs of videos.

Expensive pipelines Extensive work has been proposed to use neural networks (NNs) for ReID, advancing the accuracy steadily [58] on public datasets [14, 66]. For instance, recent pipelines cascade multiple NNs, each detecting a separate set of vehicle attributes, e.g., orientations and roof types. The additional NNs are reported to improve accuracy (mAP) by 10% with up to $7 \times$ overhead [19, 55]. We estimate that they can run no more than 15 FPS on a modern GPU.

Would cheaper features help? Cheaper NNs and vision primitives are unlikely remedies. The former were used by many *object detection* systems to provide a middle ground between high accuracy and low cost [6, 18, 29, 60]. On the much harder ReID tasks, however, modern NNs simply do not offer surplus accuracy for systems to trade off. We have tested RGB and SIFT, two cheap vision primitives for extracting object features. RGB features are highly volatile to lighting conditions and background clutter; SIFT yields poorer features compared to modern NNs, while not running significantly faster than the latter. Prepending these primitives to a ReID pipeline are likely to hurt performance.

2.4 Why is prior work inadequate

Computer vision research typically treats ReID as image retrieval [19, 38, 55, 67]. Aiming at finding all bounding boxes of a target object, computer vision studies typically focus on improving accuracy without considering query speed or efficiency much. Yet, retrieving every bounding box would miss opportunities, as we will show, that can provide useful spatiotemporal answers with much lower delays.

Existing ReID systems often consider smaller camera deployment and are evaluated on such datasets, e.g., 8 cameras over a university campus [14]. Many core designs depend on deployment-specific knowledge. For instance, ReXCam [24] searches in cameras among which spatial correlations are both strong and known. Given an input image captured by a *known* camera in the network, the system exploits camera correlation to find all images of the object. ViTrack [8] models and then predicts object trajectories in answering ReID queries. However, some assumptions (e.g., camera correlations) do not necessarily hold at the city scale; some others (e.g., a known origin camera) restrict use cases and are incompatible with the norm in ReID research [12, 13, 20, 54, 55, 68]. Without such strong assumptions, we intend our base design to be generic, and can nevertheless optimize queries with additional information as they become available (Section 7).

Spatiotemporal databases are designed for managing object trajectories, e.g., airplane movements and human movement,

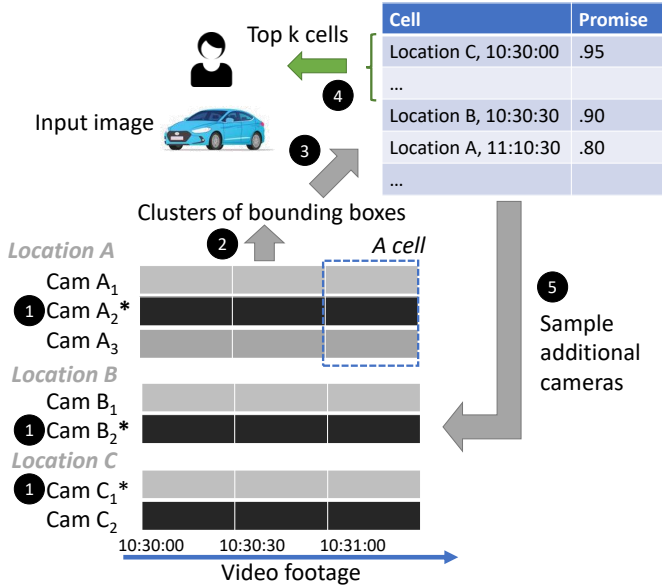


Figure 4: An overview of CLIQUE. * = a starter camera

and answering queries on them [2, 10, 21, 44, 45]. They ingest structured data, e.g., sequences of time-location tuples as from GPS; they cannot ingest unstructured video data and recognizes object occurrences as CLIQUE does. The output of our system can be the source of a spatiotemporal database.

3 CLIQUE

Video ingestion At ingestion time, CLIQUE optionally pre-processes videos from a small number of cameras, as permitted by available compute resource. The pre-processing detects objects of interesting classes (e.g., cars) and extracts their features; it is agnostic to specific queries. The pre-processing is elastic; CLIQUE will run unfinished pre-processing at the beginning of a query’s execution.

CLIQUE runs profiling as it ingests videos, a common practice of video systems [18, 24, 60]. It periodically samples videos from each camera to train several parameters used in clustering bounding boxes and determining camera sampling order. We will discuss these parameters in detail in Section 4 and 5. The profiling is light, processing 30 seconds of every 1-hour video and taking less than 10 seconds on a modern GPU.

Executing a query CLIQUE organizes all the queried video footage by cells, each consisting of video clips captured near a location during a fixed period, as shown in Figure 4.

To execute a query, CLIQUE searches in all cells iteratively; it adds cameras to each cell for processing in an incremental fashion. It starts by sampling from all cells in the query scope. The initial sampling is brief, as it only processes a small fraction of video footage in each cell – from selected

cameras (“starter cameras”) ①. From the sampled video of a cell, CLIQUE detects distinct objects out of fuzzy bounding boxes; it does so by clustering features of bounding boxes by similarity. CLIQUE treats each resultant cluster representing a distinct object, where the cluster’s centroid is an approximation of the object’s feature ②. CLIQUE ranks all the cells by their promises, estimated from similarity between their enclosed objects and the input image ③. CLIQUE emits the ranked cells as query results to the user, who reviews the top ones ④. CLIQUE selects additional cameras for processing and uses the results to update the cell list continuously ⑤. A query is terminated by the user manually (e.g., when she is satisfied with results) or when CLIQUE finishes processing videos in all queried cells.

Limitations CLIQUE inherits the statistical nature of its underpinning ReID algorithms, notably the neural networks. While CLIQUE empirically shows high confidence in its query results, e.g., it finds all true cells in more than 70% of queries (§7), it, however, cannot provide sound guarantee to do so. Similarly, although CLIQUE’s accuracy often quickly converges during query execution, there is no guarantee on the convergence rate, e.g., processing 50% of videos to reach accuracy of 0.75. The hope is that users review the top k cells for true results; they entrust CLIQUE on the remaining, unreviewed videos, being comfortable with the level of confidence that CLIQUE provides. However, in case they want to be absolutely certain that no true cells are left out, they would need to inspect all the videos.

4 Clustering bounding boxes

A core mechanism of CLIQUE is to recognize distinct objects from bounding boxes and compare the recognized objects to the input image. It addresses two concerns:

- Working around fuzzy features of bounding boxes resulted from the limitations of ReID algorithms.
- Tolerating low frame rate, which allows CLIQUE to sample more cameras, one of our principles in Section 1.

Observations on transient disturbance How to match an input image to numerous fuzzy bounding boxes, each encoding impacts of transient disturbance? The disturbance is time-varying and its impacts can be either graduate or sudden. For example, as a vehicle travels through a camera’s field of view, its bounding box may resize; its view angle may change; occasionally, it may be occluded by a light pole; its background may be intruded by another vehicle.

Key idea: clustering similar bounding boxes Disturbance to bounding box features is difficult to model and eliminate in general. Yet, if we consider similar bounding boxes in consecutive video frames, their distorted features due to graduate impacts are likely to smooth out, and the outlier features due to sudden impacts can be removed from consideration.

To this end, CLIQUE clusters object features based on their similarities. The similarities, for instance, can be measured by Euclidean distances across 1024-dimension feature vectors. As a result, each cluster represents a camera’s *general impression* on a distinct object during a given time window. The cluster’s centroid is an approximation of the camera’s ideal observation of the object.

CLIQUE’s use of clustering is novel, in that it overcomes the accuracy limitations on individual bounding boxes. Notably, it differs from prior video systems [18] that cluster objects for efficiency, e.g. to avoid processing similar objects in a cluster.

Figure 3 showcases why clustering is useful. Recall that this example shows the difficulty in comparing an input image to individual bounding boxes (Section 2). However, once we cluster the respective bounding boxes of the two vehicles, the centroids (distances as solid vertical lines) are much more robust indicators of object similarity, suggesting that the general impression of vehicle A is much closer to the input image.

In practice, we find simple clustering algorithms often suffice. CLIQUE runs k-means clustering [27] within each spatiotemporal cell. By minimizing the sum of intra-cluster variances across all clusters, k-means thus effectively puts most visually similar objects in the same cluster. k-means guarantees convergence to local optimum and is known robust to outliers [30]. We also tested other popular clustering methods, e.g., hierarchical clustering [28]. We find them less favorable than k-means, e.g., they often attribute bounding boxes of the same object to separate clusters.

Predicting the number of distinct objects (k) As a prerequisite for applying k-means in a video clip, CLIQUE must specify k as the number of distinct objects in that video. An accurate k is crucial to the clustering outcome.

CLIQUE predicts k based on a simple intuition: of a given video scene, the distinct vehicle number is correlated to the spatial density of bounding boxes. Therefore, CLIQUE only needs twofold information to predict k : (1) x_1 , the number of bounding boxes detected in the video clip; (2) x_2 , the number of frames that contain non-zero objects. Such information is already available from object detection, the ReID stage that precedes feature extraction described in Section 1. From x_1 and x_2 , CLIQUE further derives three variables as different orders of the box/frame ratio: $x_3 = (x_1/x_2)^2$, $x_4 = (x_1/x_2)$, and $x_5 = (x_2/x_1)$.

We formulate classic kernel ridge regression [53]: $k = \mathbf{ax} + b$. The model takes as an input $\mathbf{x} = [x_1, x_2, x_3, x_4, x_5]$ which consists of all aforementioned variables; its parameters are a vector \mathbf{a} and a scalar b . We instantiate one model for all the cells, for which we train a and b offline in one shot on 30-second labeled videos from 25 cameras.

Tolerance of low frame rates k-means clustering is robust to low frame rates, suiting our design principle stated in Section 1. As a comparison, we have investigated object tracking, another well-known approach to differentiating ob-

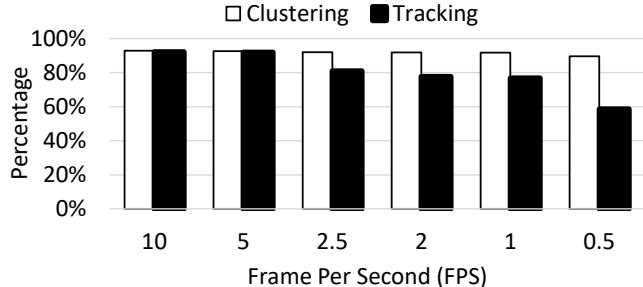


Figure 5: **Clustering of bounding boxes tolerates low frame rates.** Y-axis: the percentage of bounding boxes correctly attributed to respective objects. Object tracking implemented in OpenCV 3.4.4. Videos from CityFlow [56]

jects [32, 70]: first detecting individual bounding boxes on all frames; then linking bounding boxes across consecutive frames as distinct objects based on estimation of their motion trajectories. Yet, to estimate trajectory with good accuracy, object tracking demands a much higher frame rate than clustering. Figure 5 shows an experiment: while both k-means and object tracking can identify distinct objects well with high frame rates, e.g., 10 FPS, as the frame rate drops to 2.5 FPS or lower, object tracking quickly loses accuracy to be barely useful (~ 0.6 with 0.5 FPS). By contrast, k-means still maintains a high accuracy over 90%. Object tracking also suffers from other difficulties, e.g., differentiating multiple nearby objects following similar trajectories [1, 51].

Increasing frame rate for clustering, on the other hand, leads to a diminishing return: the accuracy improves by less than 3% by increasing from 1 to 10 FPS. This supports our principle: prioritizing camera coverage over video quality.

5 Incremental search in spatiotemporal cells

CLIQUE’s search mechanism addresses two design questions: (1) how likely does a cell contain the target object; (2) for which cells CLIQUE should process additional cameras. The former question determines the order of CLIQUE processing undecided cells and the order of CLIQUE presenting decided cells to users for review. The latter question guides CLIQUE’s search direction.

5.1 Assessing cell promises

CLIQUE estimates how likely a cell contains the target object by *promise*. The rationale is that a cell shows high promise as long as any object in this cell is highly similar to the input image. Based on this rationale, we define the *single-camera promise*, $p_{single}(R, \mathcal{C})$, as the promise CLIQUE would perceive in cell \mathcal{C} by only processing a video clip from a camera R : it is *reciprocal* to the smallest feature distance between the input and any centroid of object clusters from the video. That

is, $p_{single}(R, \mathcal{C}) = \min(\text{dist}(X, o))$ where $o \in \text{objs}$ and X is the feature of target object. As CLIQUE processes video clips from additional cameras for a cell \mathcal{C} , it estimates the cell’s overall promise, i.e., multi-camera promise, as the highest of single-camera promises of \mathcal{C} .

The promise metric reflects our intuition: a cell appears more promising to CLIQUE (with a higher multi-camera promise) as long as the cell has one strong champion camera (showing high single-camera promise) than having multiple weak supporters (medium single-camera promises).

5.2 Prioritizing cells in search

A cell’s promise reflects the single most similar object recognized in a cell. It, however, is inadequate for CLIQUE to decide whether a cell is worth further exploring, i.e., to process more cameras for the cell. To do so, CLIQUE needs to track the *accumulated* evidence discovered in the cell and the *accumulated* search efforts spent on the cell so far. Neither is reflected in the cell’s multi-camera promise. For instance, if CLIQUE only stops processing additional camera for cells with high enough promise, it may process too many cameras for cells where no single object is highly similar to the input.

To this end, CLIQUE puts all the cells in three categories:

- The green cells: CLIQUE has collected enough evidences – though not necessarily all – for them, and predicts them *likely* to contain the target object. Processing additional cameras is unlikely to change this assessment.
- The red cells: CLIQUE has collected enough evidences and predicts them *unlikely* to contain the target object. Processing additional cameras is unlikely to change this assessment.
- The gray cells: the existing evidences are insufficient. Processing one or a few cameras will likely turn the cells to red or green. This is how a human analyst would make up mind on a suspicious cell – by inspecting additional video footage from a different camera viewpoint.

Search plan All cells will begin in gray. CLIQUE navigates its search from the gray cells (to resolve the undecided cells), to the green cells (to refine the order in which they will be presented to the user), and then to the red cells (in the unlikely event of any true cells are left out). Based on new processing results in a cell, CLIQUE updates its category accordingly as will be discussed below. CLIQUE will exhaust processing cells in a category before moving to the next category. In each category, it always processes the cell that has the highest multi-camera promise.

Categorizing a cell with voting To determine the category for a cell \mathcal{C} , CLIQUE runs a simple voting mechanism to incorporating observations of multiple cameras. The voting mimics how humans would make decision out of a set of expert opinions. CLIQUE quantizes all single-camera promises with two thresholds, P_{high} and P_{low} . To \mathcal{C} , a camera with

promise p casts a high-confidence vote with a weight of 1 if $p > P_{high}$; it casts a medium-confidence vote with a weight of $1/k$ if $P_{high} < p < P_{low}$. The resultant vote count is more intuitive and tunable than, e.g., a sum of numerical single-camera promises. By tuning k , we control the relative weights of high-/medium confidence votes. In the current implementation, we sets $k=2$. That is, CLIQUE moves a cell to the green as long as CLIQUE has collected two medium-confidence votes for it.

The threshold parameters P_{high} and P_{low} hinge on the trade-off between refining existing results and exploring for new results. A lower P_{high} would eagerly put cells in the green category, postponing processing additional cameras for them until much later in the search process. By comparison, a higher P_{high} would be more reluctant in turning cells green; CLIQUE will only pause processing on them if evidence is strong.

Given that CLIQUE is a recall-oriented system to minimize human effort, we set P_{high} high so that CLIQUE continues spending resource on promising cells to refine their ranking. This is because we expect users to only inspect the top few cells; it is thus vital to include true cells in this small range. Based on the same rationale, we tune P_{low} to a low value to admit more cells to the gray category. We set $P_{high} = 1/d_{short}$, where 99% of the bounding boxes with feature distance shorter than d_{short} belong to the same vehicle. We will evaluate their sensitivity.

5.3 The search process

Stage 1: Initial sampling of cells CLIQUE starts a query by sampling from all cells and processing one camera for each.

Based on videos from the starter cameras, CLIQUE recognizes distinct objects in each cell; for each recognized object, CLIQUE derives their cluster centroids. CLIQUE may prioritize cells if heuristics is available on which cells are more likely to contain the target object, e.g., from rush hours or busier traffic intersections. As CLIQUE uses a low video frame rate (1 FPS) tolerable to the clustering algorithm (Section 4), it cover starter cameras from all cells with the lowest total cost. As initial sampling is done without information of the input image, it can be executed at the ingestion, as will be discussed below.

After processing the starter cameras for all cells in the query scope, CLIQUE has the initial categories of cells with cells in each category ranked by their promises.

Choosing starter cameras The choices matter as they set the initial direction for search. Ideally, they should be the cameras most likely to have captured the target from a viewpoint similar to the input image. In practice, one could exploit knowledge on camera deployment to help pick starter cameras, e.g., by choosing the camera that has the most similar viewpoint with the input image. Without assuming such a priori, our base design follows simple heuristics: picking cameras that has the highest density of distinct objects. The hope

is that their chances of having captured the target are higher; if the target is captured, even from a different viewpoint than the input, the resultant bounding boxes would show a decent similarity to the input and thus a high promise to CLIQUE. CLIQUE profiles each camera’s density of objects offline and picks the starter cameras ahead of query. We evaluate sensitivity of starter camera choices in Section 7.4.

Initial sampling at ingestion time Independent of input, the initial stage can be executed before queries. Pre-processing at ingestion is optional and elastic. The number of starter cameras CLIQUE can process depends on resources, e.g., the number of GPUs owned by CLIQUE. CLIQUE processes unprocessed starter cameras when a query starts, and caches the results for subsequent queries on the same scope of videos (§6).

We also consider a situation of ample resources available to ingestion. Is it worth pre-processing multiple starter cameras per geo-group? Our experiments, as will be shown in Section 7, suggest diminishing returns. This is because a small number of starter cameras properly chosen can yield sufficiently accurate cell promises and the initial ranking.

Stage 2: Incremental search Based on initial sampling of starter cameras, CLIQUE may be undecided on putting on a cell in the green or red category: the starter may completely miss the target vehicle; its viewpoint on the target vehicle may differ significantly from the input image; or the starter may have just captured a different, but visually similar vehicle.

Specifically, CLIQUE picks the next cell as follows: if the highest ranked gray cell that still has unprocessed cameras, CLIQUE processes one additional camera for it; if such gray cells are already exhausted, CLIQUE processes the highest ranked green cell that still has unprocessed cameras; if no such cells, CLIQUE moves to red cells, in hope of finding target object instances in those cells missed out previously. After selecting the next cell and processing one additional camera for it, CLIQUE updates the cell’s category and re-rank the cells. The updated categories and ranks will be CLIQUE’s basis for picking the next cell.

6 Optimizations with extra knowledge

We present the following add-on optimizations. They are based on assumptions that we intentionally left out from CLIQUE’s base design. We will evaluate them in Section 7.

Picking starter cameras based on posture similarity If the quantitative postures of deployed cameras are known to CLIQUE, e.g., as part of per camera metadata, CLIQUE can pick starter cameras as ones having the most similar postures to the origin camera. The rationale is that if the target object is captured by starter cameras, a similar viewpoint will boost the camera’s confidence. To do so, CLIQUE needs to estimate the posture of origin camera, which is different in each query. One one hand, CLIQUE may rely on human analyst to annotate

the posture (one image per query); on the other hand, it may automate the estimation with vision operators proposed by active vision research.

Sampling cameras with complementary postures In its base design, when CLIQUE samples a secondary (or subsequent) camera for a cell, it picks a random one from the same geo-group. Such decisions can be more informed by camera postures. While still keeping the choices of starter cameras, CLIQUE picks the next camera as the one that offers the most different viewpoint compared to the prior camera sampled for, i.e., the N-th camera is always the camera that has the largest viewpoint difference with the (N-1)-th camera.

Exploiting camera correlations across locations Our base design already exploits strong correlation among *co-located* cameras. In case quantitative correlations *across camera geo-groups* become available, e.g., learnt through profiling, CLIQUE can augment its strategy of ranking cells accordingly. To do so, CLIQUE requires spatial correlation, i.e., the portion of overlapped objects across geo-groups, and temporal correlations, i.e., the time range in which an object is likely to reappear in other geo-groups. Once CLIQUE identifies a high-promise cell A and moves it to the green category, CLIQUE identifies the most correlated gray cells, defined as the cells expected to share the highest portion of overlapped distinct vehicles with A, as estimated from the geo-group correlations. CLIQUE will search in these before all other gray cells. Note that CLIQUE still adds cameras to them incrementally, as in the baseline design.

Reusing states of previous queries CLIQUE speeds up a query’s execution by reusing the states from prior queries on the same videos. These queries could be fully or partially executed. Their states include all distinct objects and their features from the starter cameras, and some of bounding boxes, distinct objects, and features from the remaining cameras. To the end, CLIQUE reuses the existing distinct objects as the “free” estimation of the initial cell ranking; in incremental search, CLIQUE may favor cameras for which partial results already exist. We will evaluate the former idea experimentally.

7 Evaluation

We answer the following questions in evaluation:

§7.2 Can CLIQUE achieve good accuracy with low delays?

§7.3 Are the key designs useful?

§7.4 How is CLIQUE sensitive to its parameters and query inputs?

§7.5 How beneficial is processing at ingestion time?

§7.6 How effective are CLIQUE’s add-on optimizations?

# of all cameras	25	Total video length	25 hours
# of geo-groups	7	# of distinct vehicles	70
# of total cells	3000	# of all bounding boxes	~1M
Time duration of a cell	30 secs		

Table 1: The augmented video dataset used in evaluation

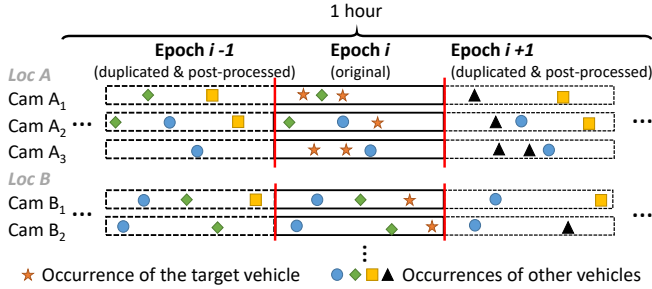


Figure 6: **Augmenting real-world city videos [56] as our test dataset:** duplicating the original epoch; erasing random vehicles from each epoch; erasing the target vehicle from all but the original epoch.

7.1 Methodology

Video Dataset An ideal video dataset for benchmarking CLIQUE would: (1) consist of long videos produced by many cameras; (2) come from real-world deployment and capture spatiotemporal patterns of vehicles; (3) have vehicle labels as the ground truth for accuracy evaluation. Real-world videos are preferred over simulators, e.g., VisualRoad [16]: while simulators can generate long traffic animations with multiple viewpoints, the resultant bounding boxes are ultimately based on vehicle motions and camera postures specified by us; it is unclear how well they reflect ReID in the real world, e.g., rarity of target objects, diverse cameras, and transient disturbance.

Unaware of such datasets in public, we use CityFlow [56] published by NVIDIA for use in the AI City Challenge 2019. The dataset consists of 5 scenarios, from which we select the largest one (scenario 4). The scenario consists of 25 cameras at 7 traffic intersections (hence 7 geo-groups) of a northern American city. The scenario includes 30 minutes of videos, capturing 17,302 vehicle bounding boxes belonging to 70 distinct vehicles. We downsample videos to 1 FPS, a low frame rate adopted in prior video systems [18, 29, 61].

We overcome a key shortcoming of the CityFlow dataset: all videos are short, each lasting around 30 seconds on a camera. We therefore augment the dataset to extend video length. To do so, we make sure to: (1) preserve the vehicle spatiotemporal patterns, within and across camera geo-groups; (2) keep the bounding boxes of target vehicles rare. Our augmenting procedure is shown in Figure 6. First, we extend each camera’s video by duplicating the original video clip as many “epochs”. Each epoch embraces videos clips from all cam-

eras; within one epoch, the original spatiotemporal patterns are preserved. Second, we remove a random fraction (0–1) of vehicles from each epoch, erasing their bounding boxes from all the video clips in that epoch. This diversifies the augmented videos over time, preventing them from becoming repeated loops of the original clips.

We further ensure that target objects are difficult to find throughout all videos. For a query with an input image of target X, we exclude the origin camera from the query scope; we erase all X’s bounding boxes from duplicated epochs while only keeping ones in the original epoch.

The final videos used in evaluation are summarized in Table 1. It spans 25 hours of videos, one hour per camera. Together, the videos consist of 3000 cells, each lasting 30 seconds; the videos include more than 1 million bounding boxes. Given a query, only 243 (0.02% of all) bounding boxes on average belong to the target vehicle, and 1.6 (0.5% of all) cells on average contain the target.

Query setup We test CLIQUE on 70 queries, each for one distinct vehicle in the video dataset. A query contains one vehicle image randomly selected from all bounding boxes of the vehicle in the dataset. We then exclude the origin camera from the query scope. As described in Section 3, a query carries no metadata, e.g., the timestamp or the origin camera of the input image, as opposed to prior work [23, 24].

Environment CLIQUE runs on a 12-core Xeon E5-2620 v3 workstation with a NVIDIA Titan V GPU. CLIQUE runs YOLO [48] to detect vehicles and ResNet-152 [17] to extract features. We train ResNet-152 on images from 329 different vehicles from 34,760 images from CityFlow [56] and Cars [31] dataset, with all vehicles used in the evaluation excluded.

Accuracy Metric We evaluate query accuracy with *recall at k*, i.e., the fraction of all true cells (i.e. containing the target object) that have been included in CLIQUE’s top k output cells. *Recall at k* is commonly used for measuring accuracy of recall-oriented retrieval focusing on rare positives [3, 5]. By setting k as low as 5, the resultant metric (*recall at 5*) measures the usefulness of query results when used with low human efforts, i.e. when a user reviews the top 5 cells returned by CLIQUE. A high value of *recall at 5* means that CLIQUE successfully returns most if not all true cells to the user, since the true cells of most queries (> 98% in our dataset) are fewer than 5.

Speed metric As CLIQUE keeps refining the rank of cells, we report the times since a query’s start until the output accuracy reaches a set of accuracy goals: 0.25, 0.50, 0.75, and 0.99.

7.2 End-to-end performance

Accuracy CLIQUE achieves high accuracy for most queries. All 70 queries achieve an average accuracy of 0.87. Among them, 65 queries (93%) meet or exceed an accuracy of 0.50;

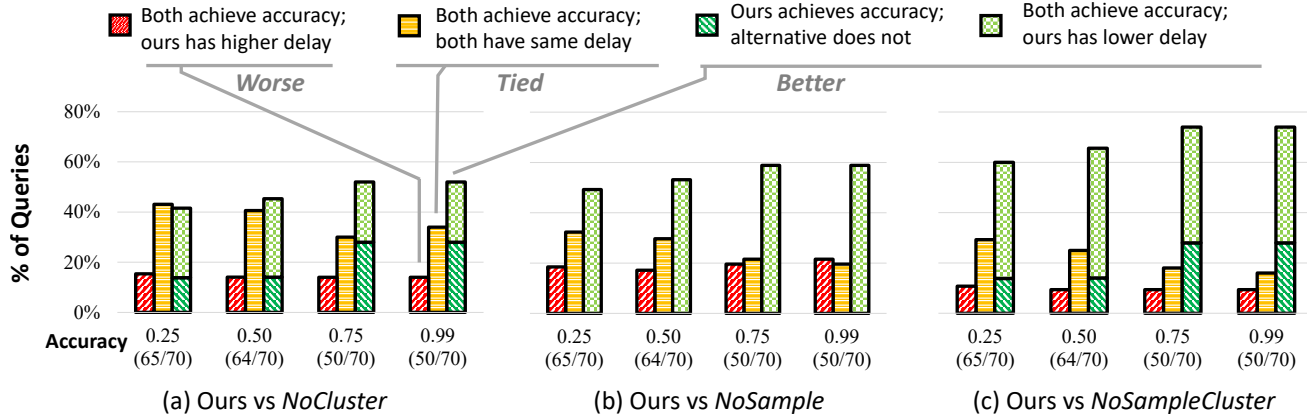


Figure 7: **Query-by-query comparison between CLIQUE and the alternatives**, broken down by per-query comparison outcomes. Numbers on bottom: accuracy goals; (X/Y): X = number of queries that CLIQUE reached the accuracy; Y = total query count

50 queries (70%) meet or exceed an accuracy of 0.99. Such accuracy is higher than what can be achieved on individual bounding boxes, as will be shown in Section 4. This validates our clustering approach: CLIQUE can make robust decisions on cells based on fuzzy bounding boxes.

We manually inspect the six queries where accuracy is low (< 0.5), attributing the root cause as the limitation of today’s feature extractors. For instance, for a query with input vehicle 262, it is challenging even for humans to associate the input image with all the 30 true bounding boxes; not surprisingly, their features show long distances to the input.

Delays CLIQUE achieves accuracy goals with moderate delays. In querying 25 hours of videos on our single-GPU machine, CLIQUE takes 59.5 seconds on average (stddev: 156.2, 90% percentile: 457.5) to reach an accuracy of 0.50, and 108.5 seconds on average (stddev: 194.9, 90% percentile: 488.0) to reach 0.99. Roughly, this speed is $830\times$ of video realtime, i.e., 4.3 seconds to perform ReID on each hour of videos.

7.3 Validation of key designs

Alternatives We compare CLIQUE to the following alternatives.

- *NoCluster*: Clustering is turned off. The alternative ranks a cell based on the minimum pairwise distance between the input image and bounding boxes in the cell. With the rank, it searches in cells by sampling from cameras as CLIQUE does.
- *NoSample*: Camera sampling is turned off. The alternative randomly picks starter cameras for each camera group. It clusters bounding boxes and ranks cells accordingly, just as CLIQUE does. Unlike CLIQUE which adds one camera to a cell and updates the cell rank, the alternative processes all cameras (in random order) for a cell before updating the rank.
- *NoSampleCluster*: Both clustering and sampling are off.

The alternative ranks a cell based on the minimum distance between the input image and bounding boxes; it processes all cameras for a cell before updating the cell rank.

Figure 7 summarizes CLIQUE’s competitiveness against the alternatives. On most queries, CLIQUE outperforms the alternatives, either reaching higher accuracy or the same accuracy in lower delays. Only on a small fraction of queries CLIQUE shows longer delays; CLIQUE never fails to reach accuracy goals attainable to the alternatives.

Clustering improves query accuracy CLIQUE’s *eventual* accuracy, i.e., the accuracy after processing all videos, reaches 0.87 averaged on all queries, while the alternatives (*NoCluster* and *NoSampleCluster*) reach 0.74 on average. The per-query accuracy gain is 0.13 on average (stddev: 0.28). Among all queries, CLIQUE’s eventual accuracy is higher on 14 out of all 70 queries; on the remaining queries CLIQUE’s accuracy ties with the above alternatives (mostly with short delays, see below) and is never lower. Clustering is vital in two ways: (1) it is robustness against outlier bounding boxes and strong disturbance, the key to achieve high accuracy goals such as 0.99; (2) based on clustering, CLIQUE’s initial cell ranking is more accurate, ensuring speedy search.

Camera sampling reduces query delays We zoom in the queries and accuracy goals attainable to CLIQUE and all the alternatives. Figure 8 shows the delay CDFs. With accuracy goals of 0.50 and 0.99, CLIQUE’s delays are $2.9\times$ and $1.7\times$ shorter than *NoCluster* on average, $4.5\times$ and $3.3\times$ shorter than *NoSample* on average, and $6.5\times$ and $3.9\times$ shorter than *NoSampleCluster* on average. The alternatives suffer from poor starter cameras which in turn result in poor initial cell ranking.

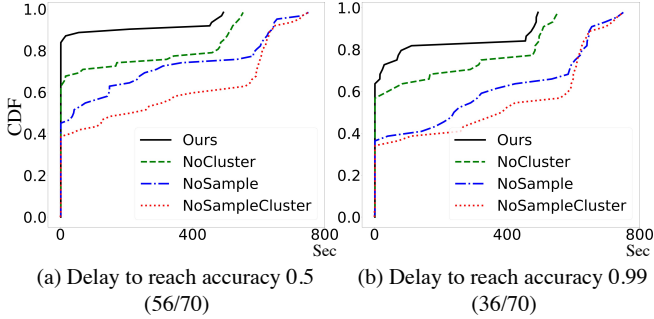


Figure 8: The CDF of query delays by CLIQUE and the alternatives. (X/Y): X = the number of queries on which all the versions reach the accuracy goal; Y = total query count

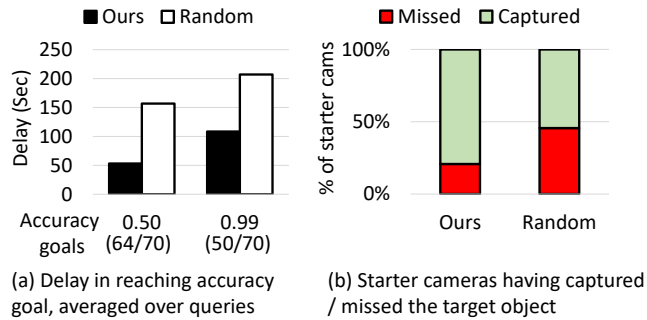


Figure 9: A comparison between CLIQUE’s choices of starter cameras and random choices. (X/Y) in (a): X = number of queries that CLIQUE reached the accuracy; Y = total query count

7.4 Sensitivity to parameters and inputs

Choices of starter cameras matter While not affecting a query’s eventual accuracy, the choice of starter cameras has a high impact on query delays. This is because the choice affects the initial rank of cells. As shown in Figure 9(a), with starter cameras randomly picked, the average query delays grow by $1.5\times$ and $3.9\times$ to meet accuracy goals of 0.50 and 0.99, respectively. Figure 9(b) shows the cause: a substantial fraction of random starter cameras miss the target vehicle they should have captured (i.e. the target captured by other camera in the same geo-group), missing opportunity in optimizing the initial ranking of cells.

Moderate sensitivity to input images CLIQUE shows resilience to different input images from our dataset. First, we replace the randomly selected input images with another random batch selected from the dataset. As a result, CLIQUE sees an average of 0.04 difference in accuracy (stddev: 0.24); it sees delay differences of 7.7 seconds (11.7%) and 13.4 seconds (12.5%) for 0.50 and 0.99, respectively. Second, we test “easier” input images by including the camera that produced the input image in a query’s scope, while still excluding the input image from the scope. As such, the query scope now

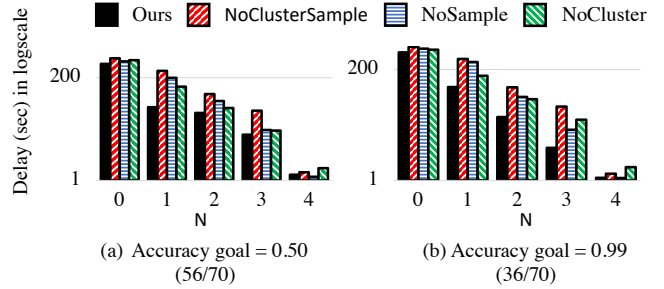


Figure 10: **Query delays with N cameras per geo-group pre-processed at ingestion time.** In case N exceeds the total cameras of a geo-group, all the cameras are pre-processed. (X/Y): X = number of queries on which **all** versions reach the accuracy goal; Y = the total query count. Y-axis in logscale.

has a camera with a viewpoint identical to the input image. CLIQUE sees moderate benefit: 0.05 higher accuracy on average (std: 0.15), 23.0% and 12.1% reduction in delays, and 1% less processed videos on average. We attribute the results to our dataset characteristics: (1) Camera redundancy: given any input image, there are likely cameras offering similar viewpoints. (2) Decent image quality. Were the input images in poorer quality, e.g., with large occlusion or low resolution, they may confuse the neural networks used in CLIQUE, resulting in lower accuracy overall.

Low sensitivity to thresholds We learn P_{high} and P_{low} via offline profiling using the original video clips. As the thresholds determine when to pause sampling cameras, their values may affect query delays but not the eventual accuracy. With methods described in (§5), we determine the default values as $P_{high}=1/d_{short}=1/0.73$ and $P_{low}=1/d_{long}=1/0.91$. We test CLIQUE by deviating from such default values, i.e., $d_{short} \pm 0.1$ and $d_{long} \pm 0.1$. Across all 70 queries, the query delays only vary by less than 10% on average. The new thresholds increase delays on more than 90% of the queries (average increase: 2.4 seconds); and reduce delays on the remaining (average reduction: 7.2 seconds). Based on the minor variation, we conclude that the default parameters are adequate; the benefit from fine tuning thresholds for individual queries are marginal.

7.5 Delay reduction by processing at ingestion

Figure 10 shows average query delays with a variety of N , the number of starter cameras per geo-group pre-processed at ingestion time. With N exceeding 4 (not shown in the Figure), CLIQUE extracts all object features in real time, leaving only feature matching (negligible overhead) to query time.

The results support lightweight preprocessing at ingestion. (1) Pre-processing starter cameras reduces query delays substantially. Comparing to no pre-processing at all, pre-processing one starter camera per group reduces query delays

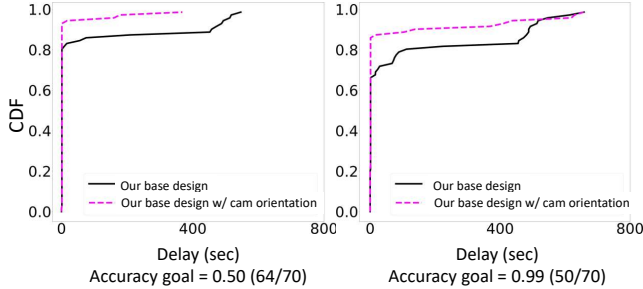


Figure 11: **Delay CDFs of CLIQUE augmented to exploit camera orientation knowledge.** (X/Y): X = number of queries that CLIQUE reached the accuracy; Y = total query count

by around $4\times$. (2) Pre-processing more than 1 starter camera per geo-group yields diminishing returns, no more than 25% delay reduction. (3) With the same pre-processing at ingestion time, CLIQUE delivers much lower delays than the alternatives.

7.6 Impact of optimizations

We evaluate the deployment-dependent optimizations (§7)

Picking starter cameras based on orientations We estimate deployed camera orientations from the map in Figure 11. We use human-labeled viewpoints for input images of queries, minimizing inaccurate viewpoints. Overall, this optimization tends to benefit queries used to be slow. On the queries used to have $\geq 70\%$ percentile delays CLIQUE sees on average $5.8\times$ and $2\times$ lower delays in reaching accuracy of 0.50 and 0.99, respectively. For the remaining 70% queries, the delay reduction is negligible as most queries converge based on starter cameras. The reason is that a significant better viewpoints from manually picked starter cameras have little impact on current well-performed queries, but on those queries that used to suffers from bad indexes. Besides, by replacing starter cameras that used to have a decent viewpoint, the initial rank of spatiotemporal cells typically does not have sharp changes, so the query delay will not differ (those $< 70\%$ percentile).

Sampling cameras by complementary orientations With camera orientations of the dataset, CLIQUE sees 4.6% and 2.0% reduction in delays to reach accuracy of 0.50 and 0.99, respectively. We identify two reasons for the minor benefit: co-located cameras are providing complementary viewpoints, and picking any of them is likely to help the search to similar degrees; the cameras with orientations opposed to the starter cameras can be inferior choices, e.g. capturing much fewer bounding boxes (and hence less likely the target object) than average cameras.

Exploiting camera correlations From the dataset, we manually derive the cross-location correlations. Assisted by the correlations, CLIQUE reduces delays by 1.7% and 1.9% reduc-

tion to reach accuracy goals of 0.50 and 0.99, respectively. The gain is insignificant due to the following reasons. At the city scale, the correlations across locations are rather weak. For instance, of any camera geo-group, only 2.4%-14.3% of the captured vehicles (mean: 8.4%) are also captured by at least half of all other geo-groups. This is much weaker than camera correlation *within* a geo-group: in our dataset, 59%-100% of vehicles are captured by more than half of the cameras within the same group; it is also weaker than what was reported on smaller camera networks [24]. As a result, the benefit from cross-location correlations is low.

Reusing states of previous queries CLIQUE can effectively speed up a new query by reusing intermediate state of previous queries. To show this, we test ten query pairs $\langle Q_{old}, Q_{new} \rangle$ on two accuracy goals of 0.50 and 0.99. The input images are randomly picked, and are different within each pair. Within each pair: we run Q_{old} , terminates it once reaching the accuracy goal, and run Q_{old} with the query state left from Q_{old} . Between pairs, we cleanse any query state. With Q_{old} reaching accuracy of 0.50 (i.e. a “brief” query), the delays for Q_{new} to reach accuracy of 0.50 and 0.99 are reduced by 86.2% and 76.8%, respectively. With Q_{old} reaching accuracy of 0.99 (i.e., a “thorough” query), the delays for Q_{new} are reduced by 86.2% and 78.1%, respectively.

8 Related Work

We discuss related work not covered previously.

Optimizing video analytics Besides ReXCam [24] and Vi-Track [8] discussed earlier, to reduce multi-camera inference cost, Caesar [36] encodes object activity correlation across cameras; Optasia [37] shares common work modules and parallelizes query plans; Jiang *et al.* [26] initiate an abstraction of camera clusters to enable resource/data sharing among cameras. There has been many works proposed to optimize video analytics with operator cascades [15, 18, 29, 52], and format tuning to trade accuracy for cost-efficiency [22, 25, 43, 61, 63]. Focus [18] saves cost by pre-processing videos with cheap NNs at ingestion. Notably, it clusters object features to avoid redundant comparisons with target objects. CLIQUE uses clustering in a different way: to smooth out transient disturbances for higher ReID accuracy. Extensive works are proposed to exploit collaborations between cloud and edge [6, 35, 46, 47, 62]; cloud/edge and mobile devices [7, 9]; cloud and cameras [59]; edge and cameras [34, 64]; and edge and drones [57]. Elf [60] imposes energy planning for counting queries on resource-frugal cameras. None above was designed for ReID queries over city-scale cameras.

Information Retrieval Recall-oriented retrievals, e.g., legal or patent search, is a group of tasks to find all relevant documents and a bad ranking typically incurs significant search efforts from domain experts [3, 5, 39]. As objects are rare in ReID tasks and typically requires domain knowledge in crime

investigation/smart traffic planning, we position CLIQUE to solve recall-oriented tasks, i.e., requiring all true cell to be retrieved, and adopt the metric of recall for evaluation.

Reconstruction of object views To estimate the object view from another viewport, prior work [69] makes attempts to estimate the per-pixel depth from a single image, but they are still far from recovering the full 3D volumetric representations from single images and cannot not explicitly estimate scene dynamics and occlusions.

9 Conclusion

We built CLIQUE, a practical object ReID engine that answers spatiotemporal queries. CLIQUE is built upon two unconventional techniques. First, CLIQUE approximates distinct objects by clustering fuzzy object features emitted by ReID algorithms before matching with the input image. Second, to search in colossal video data, CLIQUE samples cameras to maximize the spatiotemporal coverage and incrementally adds additional cameras on demand. On 25 hours of city videos spanning 25 cameras, CLIQUE on average reached an accuracy of 0.87 and runs at $830\times$ video real time in achieving high accuracy.

References

- [1] Deep learning in video multi-object tracking: A survey. *Neurocomputing*, 381:61 – 88, 2020.
- [2] Tamas Abraham and J. Roddick. Survey of spatio-temporal databases. *GeoInformatica*, 3:61–99, 1999.
- [3] Avi Arampatzis, Jaap Kamps, and Stephen Robertson. Where to stop reading a ranked list? threshold optimization using truncated score distributions. In *Proceedings of the 32nd International ACM SIGIR Conference on Research and Development in Information Retrieval, SIGIR '09*, page 524–531, New York, NY, USA, 2009. Association for Computing Machinery.
- [4] Bissan Audeh, Philippe Beaune, and Michel Beigbeder. Recall-oriented evaluation for information retrieval systems. In Mihai Lupu, Evangelos Kanoulas, and Fernando Loizides, editors, *Multidisciplinary Information Retrieval*, pages 29–32, Berlin, Heidelberg, 2013. Springer Berlin Heidelberg.
- [5] Dara Bahri, Yi Tay, Che Zheng, Donald Metzler, and Andrew Tomkins. Choppy: Cut transformer for ranked list truncation. In *Proceedings of the 43rd International ACM SIGIR Conference on Research and Development in Information Retrieval, SIGIR '20*, page 1513–1516, New York, NY, USA, 2020. Association for Computing Machinery.
- [6] Christopher Canel, Thomas Kim, Giulio Zhou, Conglong Li, Hyeontaek Lim, David G. Andersen, Michael Kaminsky, and Subramanya R. Dulloor. Scaling video analytics on constrained edge nodes. In *Proceedings of the 2nd SysML Conference*, 2019.
- [7] Tiffany Yu-Han Chen, Lenin Ravindranath, Shuo Deng, Paramvir Bahl, and Hari Balakrishnan. Glimpse: Continuous, real-time object recognition on mobile devices. In *Proceedings of the 13th ACM Conference on Embedded Networked Sensor Systems, SenSys '15*, page 155–168, New York, NY, USA, 2015. Association for Computing Machinery.
- [8] L. Cheng and J. Wang. Vitrack: Efficient tracking on the edge for commodity video surveillance systems. In *IEEE INFOCOM 2018 - IEEE Conference on Computer Communications*, pages 1052–1060, 2018.
- [9] U. Drolia, K. Guo, J. Tan, R. Gandhi, and P. Narasimhan. Cachier: Edge-caching for recognition applications. In *2017 IEEE 37th International Conference on Distributed Computing Systems (ICDCS)*, pages 276–286, 2017.
- [10] Martin Erwig, Ralf Hartmut Güting, Markus Schneider, and Michalis Vazirgiannis. Spatio-temporal data types: An approach to modeling and querying moving objects in databases. *GeoInformatica*, 3(3):269–296, September 1999.
- [11] Congress for the New Urbanism. Street networks 101. <https://www.cnu.org/our-projects/street-networks/street-networks-101>, 2020.
- [12] Yang Fu, Yunchao Wei, Guanshuo Wang, Yuqian Zhou, Honghui Shi, and Thomas S. Huang. Self-similarity grouping: A simple unsupervised cross domain adaptation approach for person re-identification. In *Proceedings of the IEEE/CVF International Conference on Computer Vision (ICCV)*, October 2019.
- [13] Yang Fu, Yunchao Wei, Yuqian Zhou, Honghui Shi, Gao Huang, Xinchao Wang, Zhiqiang Yao, and Thomas Huang. Horizontal pyramid matching for person re-identification. *Proceedings of the AAAI Conference on Artificial Intelligence*, 33(01):8295–8302, Jul. 2019.
- [14] M. Gou, S. Karanam, W. Liu, O. Camps, and R. J. Radke. Dukemtmc4reid: A large-scale multi-camera person re-identification dataset. In *2017 IEEE Conference on Computer Vision and Pattern Recognition Workshops (CVPRW)*, pages 1425–1434, July 2017.

- [15] Seungyeop Han, Haichen Shen, Matthai Philipose, Sharad Agarwal, Alec Wolman, and Arvind Krishnamurthy. Mcdnn: An approximation-based execution framework for deep stream processing under resource constraints. In Proceedings of the 14th Annual International Conference on Mobile Systems, Applications, and Services, MobiSys '16, pages 123–136, New York, NY, USA, 2016. ACM.
- [16] Brandon Haynes, Amrita Mazumdar, Magdalena Balazinska, Luis Ceze, and Alvin Cheung. Visual road: A video data management benchmark. In SIGMOD, pages 972–987, 2019.
- [17] K. He, X. Zhang, S. Ren, and J. Sun. Deep residual learning for image recognition. In 2016 IEEE Conference on Computer Vision and Pattern Recognition (CVPR), pages 770–778, 2016.
- [18] Kevin Hsieh, Ganesh Ananthanarayanan, Peter Bodik, Shivaram Venkataraman, Paramvir Bahl, Matthai Philipose, Phillip B. Gibbons, and Onur Mutlu. Focus: Querying large video datasets with low latency and low cost. In 13th USENIX Symposium on Operating Systems Design and Implementation (OSDI 18), Carlsbad, CA, 2018. USENIX Association.
- [19] De-An Huang, Vignesh Ramanathan, Dhruv Mahajan, Manohar Paluri, Li Fei-Fei, and Juan Carlos Niebles. What makes a video a video: Analyzing temporal information in video understanding models and datasets. In CVPR, pages 7366–7375. IEEE Computer Society, 2018.
- [20] Tsung-Wei Huang, Jiarui Cai, Hao Yang, Hung-Min Hsu, and Jenq-Neng Hwang. Multi-view vehicle re-identification using temporal attention model and metadata re-ranking. In Proceedings of the IEEE/CVF Conference on Computer Vision and Pattern Recognition (CVPR) Workshops, June 2019.
- [21] James N. Hughes, Andrew Annex, Christopher N. Eichelberger, Anthony Fox, Andrew Hulbert, and Michael Ronquest. GeoMesa: a distributed architecture for spatio-temporal fusion. In Matthew F. Pallechia, Kannappan Palaniappan, Peter J. Doucette, Shiloh L. Dockstader, Gunasekaran Seetharaman, and Paul B. Deignan, editors, Geospatial Informatics, Fusion, and Motion Video Analytics V, volume 9473, pages 128–140. International Society for Optics and Photonics, SPIE, 2015.
- [22] Chien-Chun Hung, Ganesh Ananthanarayanan, Peter Bodik, Leana Golubchik, Minlan Yu, Victor Bahl, and Matthai Philipose. Videoege: Processing camera streams using hierarchical clusters. October 2018.
- [23] Samvit Jain, Ganesh Ananthanarayanan, Junchen Jiang, Yuanchao Shu, and Joseph E Gonzalez. Scaling video analytics systems to large camera deployments. arXiv preprint arXiv:1809.02318, 2018.
- [24] Samvit Jain, Junchen Jiang, Yuanchao Shu, Ganesh Ananthanarayanan, and Joseph Gonzalez. Rexcam: Resource-efficient, cross-camera video analytics at enterprise scale. CoRR, abs/1811.01268, 2018.
- [25] Junchen Jiang, Ganesh Ananthanarayanan, Peter Bodik, Siddhartha Sen, and Ion Stoica. Chameleon: Scalable adaptation of video analytics. In Proceedings of the 2018 Conference of the ACM Special Interest Group on Data Communication, SIGCOMM '18, pages 253–266, New York, NY, USA, 2018. ACM.
- [26] Junchen Jiang, Yuhao Zhou, Ganesh Ananthanarayanan, Yuanchao Shu, and Andrew A. Chien. Networked cameras are the new big data clusters. In Proceedings of the 2019 Workshop on Hot Topics in Video Analytics and Intelligent Edges, HotEdgeVideo'19, page 1–7, New York, NY, USA, 2019. Association for Computing Machinery.
- [27] Xin Jin and Jiawei Han. K-Means Clustering, pages 563–564. Springer US, Boston, MA, 2010.
- [28] S. C. Johnson. Hierarchical clustering schemes. Psychometrika, 32:241–254, 1967.
- [29] Daniel Kang, John Emmons, Firas Abuzaid, Peter Bailis, and Matei Zaharia. Noscope: Optimizing neural network queries over video at scale. Proc. VLDB Endow., 10(11):1586–1597, August 2017.
- [30] Tapas Kanungo, David M. Mount, Nathan S. Netanyahu, Christine D. Piatko, Ruth Silverman, and Angela Y. Wu. An efficient k-means clustering algorithm: Analysis and implementation. 24(7), 2002.
- [31] Jonathan Krause, Michael Stark, Jia Deng, and Li Fei-Fei. 3d object representations for fine-grained categorization. ICCVW '13, page 554–561, USA, 2013. IEEE Computer Society.
- [32] B. Li, J. Yan, W. Wu, Z. Zhu, and X. Hu. High performance visual tracking with siamese region proposal network. In 2018 IEEE/CVF Conference on Computer Vision and Pattern Recognition, pages 8971–8980, 2018.
- [33] Xiyang Li and Zhihao Zhou. Object Re-Identification Based on Deep Learning. 06 2019.
- [34] Yuanqi Li, Arthi Padmanabhan, Pengzhan Zhao, Yufei Wang, Guoqing Harry Xu, and Ravi Netravali. Reducto: On-camera filtering for resource-efficient

- real-time video analytics. In Proceedings of the Annual Conference of the ACM Special Interest Group on Data Communication on the Applications, Technologies, Architectures, and Protocols for Computer Communication, SIGCOMM '20, page 359–376, New York, NY, USA, 2020. Association for Computing Machinery.
- [35] Peng Liu, Bozhao Qi, and Suman Banerjee. Edge-eye: An edge service framework for real-time intelligent video analytics. In Proceedings of the 1st International Workshop on Edge Systems, Analytics and Networking, EdgeSys'18, pages 1–6, New York, NY, USA, 2018. ACM.
- [36] Xiaochen Liu, Pradipta Ghosh, Oytun Ulutan, B. S. Manjunath, Kevin Chan, and Ramesh Govindan. Caesar: Cross-camera complex activity recognition. In Proceedings of the 17th Conference on Embedded Networked Sensor Systems, SenSys '19, page 232–244, New York, NY, USA, 2019. Association for Computing Machinery.
- [37] Yao Lu, Aakanksha Chowdhery, and Srikanth Kandula. Optasia: A relational platform for efficient large-scale video analytics. In Proceedings of the Seventh ACM Symposium on Cloud Computing, SoCC '16, page 57–70, New York, NY, USA, 2016. Association for Computing Machinery.
- [38] Kai Lv, Heming Du, Yunzhong Hou, Weijian Deng, Hao Sheng, Jianbin Jiao, and Liang Zheng. Vehicle re-identification with location and time stamps. In Proceedings of the IEEE/CVF Conference on Computer Vision and Pattern Recognition (CVPR) Workshops, June 2019.
- [39] Walid Magdy and Gareth J.F. Jones. Pres: A score metric for evaluating recall-oriented information retrieval applications. In Proceedings of the 33rd International ACM SIGIR Conference on Research and Development in Information Retrieval, SIGIR '10, page 611–618, New York, NY, USA, 2010. Association for Computing Machinery.
- [40] Wolfram MathWorld. l^2 -norm. <https://mathworld.wolfram.com/L2-Norm.html>, 2020.
- [41] Microsoft. Video analytics towards vision zero, 2019.
- [42] Milind Naphade, Rama Chellappa, David Anastasiu, Anuj Sharma, Ming-Ching Chang, Xiaodong Yang, Shuo Wang, Zheng Tang, and Liang Zheng. Ai city challenge, 2020.
- [43] Chrisma Pakha, Aakanksha Chowdhery, and Junchen Jiang. Reinventing video streaming for distributed vision analytics. In 10th USENIX Workshop on Hot Topics in Cloud Computing (HotCloud 18), Boston, MA, 2018. USENIX Association.
- [44] Neelabh Pant, Mohammadhani Fouladgar, Ramez Elmasri, and Kulsawasd Jitkajornwanich. A survey of spatio-temporal database research. In Ngoc Thanh Nguyen, Duong Hung Hoang, Tzung-Pei Hong, Hoang Pham, and Bogdan Trawiński, editors, Intelligent Information and Database Systems, pages 115–126, Cham, 2018. Springer International Publishing.
- [45] Kriengkrai Porkaew, Iosif Lazaridis, and Sharad Mehrotra. Querying mobile objects in spatio-temporal databases. In Christian S. Jensen, Markus Schneider, Bernhard Seeger, and Vassilis J. Tsotras, editors, Advances in Spatial and Temporal Databases, pages 59–78, Berlin, Heidelberg, 2001. Springer Berlin Heidelberg.
- [46] X. Ran, H. Chen, X. Zhu, Z. Liu, and J. Chen. Deepdecision: A mobile deep learning framework for edge video analytics. In IEEE INFOCOM 2018 - IEEE Conference on Computer Communications, pages 1421–1429, April 2018.
- [47] Arun Ravindran and Anjus George. An edge datastore architecture for latency-critical distributed machine vision applications. In USENIX Workshop on Hot Topics in Edge Computing (HotEdge 18), Boston, MA, July 2018. USENIX Association.
- [48] J. Redmon, S. Divvala, R. Girshick, and A. Farhadi. You only look once: Unified, real-time object detection. In 2016 IEEE Conference on Computer Vision and Pattern Recognition (CVPR), pages 779–788, June 2016.
- [49] Joseph Redmon and Ali Farhadi. Yolo: Real-time object detection, 2016.
- [50] Joseph Redmon and Ali Farhadi. Yolo9000: Better, faster, stronger. [arXiv preprint arXiv:1612.08242](https://arxiv.org/abs/1612.08242), 2016.
- [51] Deval Shah. The surveillance phenomenon you must know about : Multi object tracking. <https://medium.com/visionwizard/object-tracking-675d7a33e687>, 2020.
- [52] Haichen Shen, Seungyeop Han, Matthai Philipose, and Arvind Krishnamurthy. Fast video classification via adaptive cascading of deep models. In The IEEE Conference on Computer Vision and Pattern Recognition (CVPR), July 2017.
- [53] sklearn. Kernel ridge regression, 2020.

- [54] Yifan Sun, Liang Zheng, Yi Yang, Qi Tian, and Shengjin Wang. Beyond part models: Person retrieval with refined part pooling (and a strong convolutional baseline). In Proceedings of the European Conference on Computer Vision (ECCV), September 2018.
- [55] Xiao Tan, Zhigang Wang, Minyue Jiang, Xipeng Yang, Jian Wang, Yuan Gao, Xiangbo Su, Xiaoqing Ye, Yuchen Yuan, Dongliang He, Shilei Wen, and Errui Ding. Multi-camera vehicle tracking and re-identification based on visual and spatial-temporal features. In The IEEE Conference on Computer Vision and Pattern Recognition (CVPR) Workshops, June 2019.
- [56] Zheng Tang, Milind Naphade, Ming-Yu Liu, Xiaodong Yang, Stan Birchfield, Shuo Wang, Ratnesh Kumar, David Anastasiu, and Jenq-Neng Hwang. Cityflow: A city-scale benchmark for multi-target multi-camera vehicle tracking and re-identification. In The IEEE Conference on Computer Vision and Pattern Recognition (CVPR), June 2019.
- [57] Junjue Wang, Ziqiang Feng, Zhuo Chen, Shilpa George, Mihir Bala, Padmanabhan Pillai, Shao-Wen Yang, and Mahadev Satyanarayanan. Bandwidth-efficient live video analytics for drones via edge computing. In 2018 IEEE/ACM Symposium on Edge Computing, SEC 2018, Seattle, WA, USA, October 25-27, 2018, pages 159–173, 2018.
- [58] Paper with code. Person re-identification on dukemtmc-reid, 2020.
- [59] Mengwei Xu, Tiantu Xu, Yunxin Liu, Xuanzhe Liu, Gang Huang, and Felix Xiaozhu Lin. Supporting video queries on zero-streaming cameras. CoRR, abs/1904.12342, 2019.
- [60] Mengwei Xu, Xiwen Zhang, Yunxin Liu, Gang Huang, Xuanzhe Liu, and Felix Xiaozhu Lin. Approximate query service on autonomous iot cameras. In Proceedings of the 18th International Conference on Mobile Systems, Applications, and Services, MobiSys '20, page 191–205, New York, NY, USA, 2020. Association for Computing Machinery.
- [61] Tiantu Xu, Luis Materon Botelho, and Felix Xiaozhu Lin. Vstore: A data store for analytics on large videos. In Proceedings of the Fourteenth EuroSys Conference 2019, EuroSys '19, pages 16:1–16:17, New York, NY, USA, 2019. ACM.
- [62] S. Yi, Z. Hao, Q. Zhang, Q. Zhang, W. Shi, and Q. Li. Lavea: Latency-aware video analytics on edge computing platform. In 2017 IEEE 37th International Conference on Distributed Computing Systems (ICDCS), pages 2573–2574, June 2017.
- [63] Haoyu Zhang, Ganesh Ananthanarayanan, Peter Bodik, Matthai Philipose, Paramvir Bahl, and Michael J. Freedman. Live video analytics at scale with approximation and delay-tolerance. In 14th USENIX Symposium on Networked Systems Design and Implementation (NSDI 17), pages 377–392, Boston, MA, 2017. USENIX Association.
- [64] Tan Zhang, Aakanksha Chowdhery, Paramvir (Victor) Bahl, Kyle Jamieson, and Suman Banerjee. The design and implementation of a wireless video surveillance system. In Proceedings of the 21st Annual International Conference on Mobile Computing and Networking, MobiCom '15, pages 426–438, New York, NY, USA, 2015. ACM.
- [65] L. Zheng, L. Shen, L. Tian, S. Wang, J. Wang, and Q. Tian. Scalable person re-identification: A benchmark. In 2015 IEEE International Conference on Computer Vision (ICCV), pages 1116–1124, 2015.
- [66] L. Zheng, L. Shen, L. Tian, S. Wang, J. Wang, and Q. Tian. Scalable person re-identification: A benchmark. In 2015 IEEE International Conference on Computer Vision (ICCV), pages 1116–1124, 2015.
- [67] Liang Zheng, Yi Yang, and Alexander G. Hauptmann. Person re-identification: Past, present and future. CoRR, abs/1610.02984, 2016.
- [68] Z. Zhong, L. Zheng, D. Cao, and S. Li. Re-ranking person re-identification with k-reciprocal encoding. In 2017 IEEE Conference on Computer Vision and Pattern Recognition (CVPR), pages 3652–3661, 2017.
- [69] T. Zhou, M. Brown, N. Snavely, and D. G. Lowe. Unsupervised learning of depth and ego-motion from video. In 2017 IEEE Conference on Computer Vision and Pattern Recognition (CVPR), pages 6612–6619, 2017.
- [70] Zheng Zhu, Qiang Wang, Bo Li, Wei Wu, Junjie Yan, and Weiming Hu. Distractor-aware siamese networks for visual object tracking. In Proceedings of the European Conference on Computer Vision (ECCV), September 2018.